euspen's 19th International Conference & Exhibition, Bilbao, ES, June 2019
www.euspen.eu

Design of a large stroke flexure-based suspension for an iron core torque motor

M. Naves, M. Nijenhuis, W.B.J. Hakvoort, D.M. Brouwer

University of Twente, Enschede, The Netherlands

m.naves@utwente.nl

Abstract
Iron core torque motors provide a high power density, but require high off-axis stiffness, which is normally too demanding for flexure mechanisms especially when considering large range of motion applications. In this paper, a flexure-based suspension for a high torque iron core direct drive torque motor with a large range of motion of 60 degrees is presented. This flexure-based suspension provides the required high radial stiffness (>1000N/mm) combined with a high radial load capacity (500N) over the full range of motion. Furthermore, the suspension maintains a constant position of the pivot axis within 0.1mm, which is required to limit pull-in forces and to stay within alignment tolerances of the actuator. A prototype has been designed and constructed and experimental validations confirm the high radial stiffness and load capacity of the rotor suspension.

Keywords: Compliant mechanisms, large stroke, iron core motor, flexure mechanisms

1. Introduction

In high precision applications, flexure-based mechanisms are used for their deterministic behavior due to the absence of play and friction. To maintain these deterministic properties, the actuators of flexure-based precision systems should also be free of play and friction. To this end, direct drive actuators are often used since they do not rely on tribological contacts. Common Lorentz-type actuators such as voice coil, linear iron-less or rotary iron-less (torque) motors rely on a permanent magnetic field and coil windings (without iron core) to provide actuation forces. Due to the abscence of the iron core, disruptive cogging and high parasitic magnetic forces are avoided. However, the absence of the iron core also results in a reduced strength of the magnetic field and reduced thermal dissipation, which decreases the maximum actuation force. Therefore, iron-less actuators are not always able to provide sufficient actuation force for demanding applications.

In contrast, Lorentz-type actuators with an iron core, in which the coils are mounted in an iron lamination stack, have actuation forces that are up to a factor of two larger [1], though at the expense of parasitic magnetic forces. These parasitic forces are proportional with the mis-alignment between the magnet track and iron core away from the equilibrium position, resulting in a destabilizing negative stiffness. To counteract for this negative stiffness, a stiff bearing construction is required, which is often too demanding for flexure mechanisms due to their limited support stiffness especially when considering large range of motion applications [2]. Furthermore, large stroke flexure mechanisms often suffer from a limit load capacity, insufficient for the resulting reaction forces on the bearing construction.

Additionally, the non-linear nature of the elastic deformations of the flexures also results in parasitic motion [3] that easily exceeds the alignment tolerances of typical actuators, because the airgap between the magnet track and coil is often small. Furthermore, due to the negative stiffness provided by the iron core, parasitic motion results in additional parasitic forces.

In this paper, a flexure-based rotary actuator suspension with 60 degrees range of motion for use in a fully flexure-based high precision hexapod system is presented. The actuator suspension provides the required high radial support stiffness, high load capacity and near constant position of the pivot axis in order to bear a high torque iron core direct drive torque motor that can provide an ultimate torque of 55Nm. For the design of the suspension, three different flexure joint topologies are optimized and compared in terms of shift of the rotation axis, load capacity and radial support stiffness. A prototype of the optimal flexure-based actuator suspension has been designed, built and validated.

2. Motor selection

The direct drive torque motor considered in this paper is Tecnotion's direct drive QTR-A-133-60 motor [4]. This actuator is able to meet the torque requirements for the hexapod application, allowing for accelerations up to 10G. Furthermore, it allows for a continuous torque of 21.9Nm and an ultimate torque[1] of 55.5Nm. The negative radial stiffness caused by the iron core is approximately 350 N/mm and a radial alignment of <1mm is required to prevent contact between the rotor and stator.

3. Flexure hinge topologies

For the considered hexapod system, a repeatability of under 1µrad of the actuator position is demanded to allow for precise positioning of the end-effector. To meet this requirement, a flexure based actuator suspension is used to obtain the required deterministic behavior and to eliminate sources of play and friction. A commonly used flexure hinge design is the three flexure cross hinge (TFCH), also known as a cross spring

[1] *At ultimate torque the temperature of the coil increases by 20C°/s. The maximum duration at which this torque can be maintained depends on thermal properties of the coil housing*

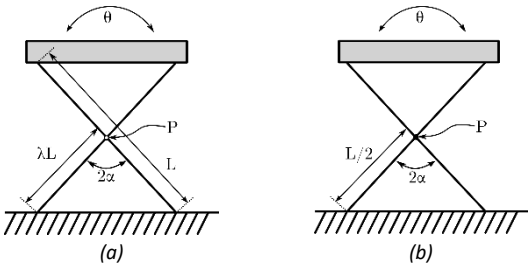

Figure 1. Schematic illustration of the (a) Three flexure Cross Hinge and (b) Cartwheel flexure hinge

$$P_{TFCH} = \frac{-9\lambda^2 + 9\lambda - 1}{15\cos(\alpha)}\theta^2 L \qquad (1)$$

pivot, which consists of three separate leafsprings. A schematic overview of the TFCH is provided in figure 1a. Shift of the pivot axis (P) of the TFCH as a function of the deflection angle (θ) is given by equation 1 [3].

From the numerator it can be concluded that the typically used value of $\lambda = 0.5$ (the leafsprings cross at half their length) results in a relatively large shift of the pivot axis, which easily exceeds the allowed 1mm. As an alternative, the pivot shift can be reduced to a minimum by choosing $\lambda = 1/2 \pm \sqrt{5}/6$. Although this specific choice for λ greatly reduces pivot shift, the asymmetric design results in high stress concentrations requiring a smaller thickness of the flexures for the same stress limit. Consequently, support stiffness and load capacity are strongly reduced.

An alternative flexure hinge design is provided by the cartwheel flexure hinge (CFH) [5], which consists of four leafsprings connected to each other at the center (P). A schematic overview of the CFH is provided in figure 1b. Shift of the pivot axis, which effectively consists of two cross spring pivots with $\lambda = 1$ stacked in series, is provided by equation 2. Hereby, shift of the pivot axis is reduced by a factor of approximately five compared to the TFCH considering $\lambda = 0.5$.

$$P_{CFH} = -\frac{1}{60\cos(\alpha)}L\theta^2 \qquad (2)$$

Lastly, the butterfly hinge (BFH) [6] is considered, schematically illustrated in figure 2a. The BFH effectively consists of four cross spring pivots stacked in series with $\lambda \approx 1$ where the shift of the pivot axis can be deducted from equation 1, resulting in:

$$P_{BFH} = \frac{(9\lambda^2 - 9\lambda + 1)(\cos(\alpha_2) - \cos(\alpha_1))}{240\cos(\alpha_1)\cos(\alpha_2)}L\theta^2 \qquad (3)$$

Due to symmetry in its design, shift of the pivot axis of the four leafsprings connected to the fixed world and end-effector are opposite to the shift of the four leafsprings connected to the central intermediate body, partially canceling out its pivot shift. This provides a reduction in pivot shift of approximately a factor of 25 with respect to the TFCH for typical values of λ and α. To reduce pivot shift even further, the dimensioning (i.e. the length and relative position at which the leafsprings cross the rotation axis) of the leafsprings can be chosen independently. This way, the combined pivot shift can be reduced to near zero.

For the BFH, it has to be noted that each intermediate body has an unintended rotational degree of freedom around the rotation axis of the joint, introducing three underconstrained degrees of freedom. For most flexure-based mechanisms,

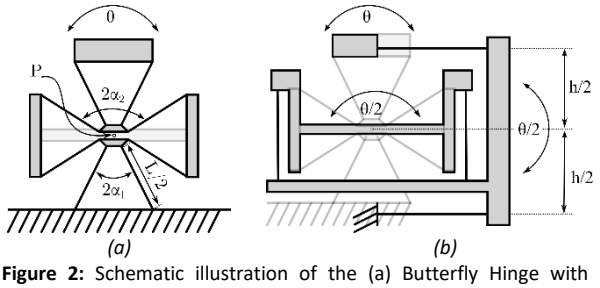

Figure 2: Schematic illustration of the (a) Butterfly Hinge with (b) slaving mechanism [6]

under-constrained intermediate bodies dramatically deteriorate support stiffness (especially for large deflection angles) due to the coupling between external loads applied on the end-effector and the underconstrained degrees of freedom of the intermediate bodies, similar to the compounded parallel leafspring guidance without slaving mechanism [7]. However, as the instant center of rotation of each intermediate body and the end-effector coincide and hardly vary, external loads on the end-effector do not result in a reaction moment in the degrees of freedom of the intermediate body. Due to this property, support stiffness is not impaired by the underconstraints.

However, with respect to the dynamic behavior of the joint, the underconstrained intermediate bodies can result in unwanted vibrations of the system. The two small intermediate bodies positioned between the first and second set of leafsprings and the third and fourth set of leafsprings have a high natural frequency in the underconstrained degree of freedom due to the low amount of inertia with respect to the rotation axis of the joint. Therefore, these underconstrained degrees of freedom typically do not introduce unwanted vibrations in the frequency range of interest. The large intermediate body positioned between the second and third flexure set does potentially lead to unwanted vibrations due to its relatively large size and consequently its high inertia. In order to eliminate this underconstraint, an additional slaving mechanism can be added which couples motion of the end-effector and the intermediate body with a two-to-one ratio [6]. A schematic overview of a butterfly hinge with slaving mechanism is provided in figure 2b.

4. Shape optimization

In order to compare the support stiffness and load capacity of the hinge topologies described in the previous section in addition to shift of the pivot axis, an adapted Nelder-Mead based shape optimization algorithm [8] is used to optimize the designs for radial support stiffness. In this optimization, the performance is evaluated over the entire range of motion with the flexible multi-body software SPACAR [9]. In SPACAR, all leafsprings are modeled as a series of interconnected nonlinear 3D finite beam elements which includes geometric non-linearities. Flexibility of these elements is naturally accounted for in the formulation owing to a specific choice of so-called discrete deformation modes. This way, only a limited number of elements are required to produce both fast and accurate results.

The objective of the optimization is to maximize the radial (off-axis) stiffness in the most compliant direction over the range of motion of 60 degrees (K_{crit}). As material, we select tool steel where we limit the allowable stress to 600MPa, which is about 40% of the yield stress of the material. The total width of the hinges is limited to 100mm measured in the direction of the rotation axis.

Table 1: *Optimization results of the shape optimization. The critical radial support stiffness (K_{crit}), critical load capacity (F_{crit}) and pivot shift (P_{shift}) is provided for the maximum deflection angle of $\theta = 30°$.*

	TFCH	TFCH	CFH	BFH	BFH*
λ	0.5	0.87	1	1.07	1.07,1.11*
L [mm]	60	63	153	70	70,79*
t [mm]	0.53	0.20	0.42	0.33	0.33
α (α_1) [deg]	45		45	35	35
α_2 [deg]	-	-	-	55	55
K_{crit} [N/mm]	1454	56	837	1513	1141
F_{crit} [N]	-	-	75	500	490
P_{shift} [mm]	1.89	0.09	0.94	0.08	0.01

**Butterfly hinge optimized for minimal pivot shift with L and λ chosen independently for each set of leafsprings*

An overview of the optimization results in presented in table 1, at which the design parameters are defined according to figure 1 and 2 and with t indicating the thickness of the flexures. Furthermore, the critical load capacity of the elastic hinges is limited by their finite radial support stiffness, causing contact between the rotor and stator for excessive loads. Therefore, the critical load capacity (F_{crit}) is defined as the load at which shift in the position of the rotor exceeds 1mm. For evaluation of the critical load capacity, the decrease in radial support stiffness for increasing loads and the negative stiffness caused by the iron core is taken into account. Lastly, pivot shift caused by the non-linear nature of the deformations without considering external loads is provided by P_{shift}.

From these results it can be concluded that the traditional TFCH with $\lambda = 0.5$ does not maintain the position of the pivot-axis within the required 1mm. Pivot shift can be reduced by choosing $\lambda = 1/2 + \sqrt{5}/6 \approx 0.87$. However, the assymmetric design which results in high stress concentrations requires flexures with small thickness, resulting in insufficient support stiffness and load capacity to bear the rotor. An intermediate solution is provided by the CFH, which provides mediocre support stiffness and shift of the pivot axis, although only providing a limited load capacity. Highest performance is obtained with the BFH which provides both a low shift of the pivot axis, high support stiffness and high load capacity.

Figure 4: Photograph of the constructed prototype

Furthermore, pivot shift of the BFH can be reduced to almost zero by optimizing the geometry of each individual set of leafsprings in the BFH for minimal pivot shift. However, this comes at the cost of reduced support stiffness due to the increased value of L and λ required to cancel out pivot shift of each individual stage.

5. Prototype design

Based on the optimization results, a prototype of a flexible actuator suspension for the selected torque motor is constructed. For this purpose, the butterfly hinge with equal length for each leafspring is selected as it provides the highest level of support stiffness and load capacity and as pivot shift is sufficiently small to maintain proper alignment of the rotor over the full range of motion. An exploded view of the prototype is provided in figure 3, which shows the suspension for two actuators with parallel rotation axes.

In the design, two butterfly hinges (1) with a width of 50mm and slaving mechanism (2) are placed on each side of an aluminum rotor hub (3) which carries the rotor (4). The central ``large'' intermediate bodies (5) which are slaved by the slaving mechanisms are interconnected with an aluminum body (6). This body is placed inside the rotor hub and provides a stiff connection between the intermediate slaved bodies. Furthermore, a linear encoder (7) is placed on the rotor hub (concentric with the rotor) to provide sensing of the rotor position and a mechanical stop (8) and optical switch (9) are

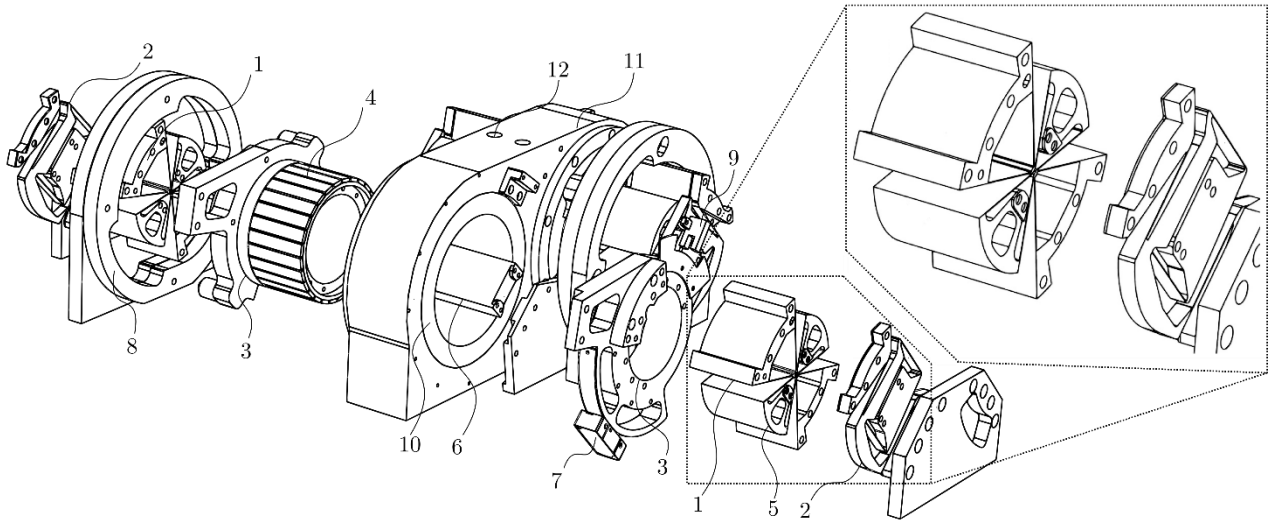

Figure 3: Exploded view of actuator suspension. 1) Butterfly hinge 2) Slaving mechanism 3) Rotor-hub 4) Rotor 5) Slaved intermediate body 6) Body coupling intermediate bodies of the butterfly hinges 7) Encoder 8) Mechanical stop 9) Optical switch 10) Stator 11) Stator housing 12) Cooling channels.

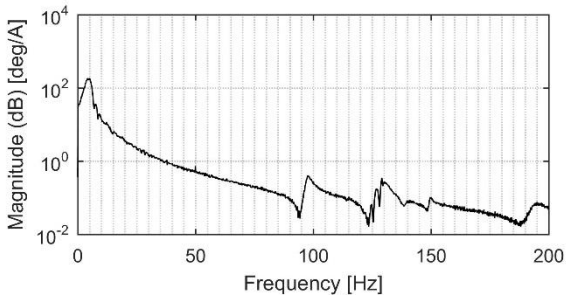

Figure 5: Frequency response from actuator current (A) to rotor position (deg)

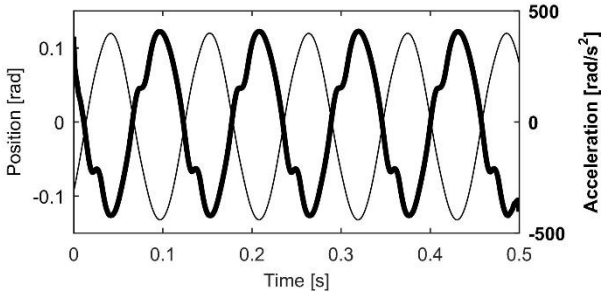

Figure 6: Measured postion and acceleration of the rotor during loadability tests

added to prevent excessive rotation of the rotor. The stationary part of the actuator containing the coils, the stator (10), is fixed inside an aluminum frame (11). This frame holds the stator and improves the thermal dissipation for the actuator. Furthermore, the housing is equipped with cooling channels (12) to add active cooling to the stator for high load applications. A photograph of the realized prototype is provided in figure 4. It has to be noted that insertion of the rotor during assembly requires special attention and additional assembly tools to provide resistance to the negative radial stiffness and to ensure good alignment between the stator and rotor.

6. Experimental validation

The first crucial property off the actuator suspension is the radial support stiffness at maximum deflection angle. This support stiffness is directly related to the frequency of the first parasitic vibration mode of the end-effector and is therefore used to validate its support stiffness. The parasitic vibration mode consists of a translational radial motion which can be sensed by the encoder on the rotor-hub. To determine the stiffness, the frequency response from actuator current to rotation of the rotor is determined, which is provided in figure 5. This frequency response is evaluated close to the maximum deflection angle while still allowing for sufficient range of motion for a sweep signal on the input current. From this data, the first parasitic frequency can be clearly observed at 98Hz. In combination with a 2.9kg mass of the end-effector, consisting of the rotor, rotor-hub and a part of the butterfly hinges, this provides an radial support stiffness of approximately 1100 N/mm. When also taking into account the negative stiffness induced by the rotor, the resulting support stiffness from the elastic suspension equals 1450N/mm. The slightly lower value in support stiffness can be related to additional compliance in the frame parts which are considered rigid in simulations. However, measured support stiffness is still in good agreement with simulations and confirm the high radial stiffness of the butterfly hinges.

To validate the load capacity, an additional off-centered mass is attached to the rotor which corresponds to the load in the hexapod application. This load provides an inertia of 0.066kgm^2 with respect to the rotation axis and a mass of 4.4kg with the center of mass located at 65mm from the axis of rotation. Radial forces are generated by accelerating the mass up to 400 rad/s^2, resulting in reaction forces of approximately 115N (23% of F_{crit}). The measured position and acceleration is presented in figure 6. Visual inspection of the rotor suspension during the tests show no failure or parasitic deformations which indicate the actuator suspension is able to wisthand the resulting reaction forces. Note the repeating ripple in accelerations in figure 6 is caused by cogging forces of the actuator.

7. Conclusion

A high performance flexure-based suspension for an iron core direct drive torque motor with high radial support stiffness, high load capacity and 60 degrees range of motion has been designed. For the suspension, a butterfly hinge design has been used which features less then 0.1mm shift of the pivot axis, limiting pull-in forces typical for iron core actuators. Optimizations on the butterfly hinge design have resulted in an actuator suspensions with a radial support stiffness exceeding 1000N/mm and a load capacity of 500N, providing adequate support stiffness to compensate for the negative stiffness induced by the iron core of the actuator. Experimental validations confirm the high support stiffness and load capacity and prove the applicability of a flexure-based suspension for high torque iron core actuators.

Acknowledgement

This research was funded by the Innovative Research Incentives Scheme VIDI (Stichting voor de Technische Wetenschappen)(14152 NOW TTW) of the ministry of Education, Culture and Sciense of the Netherlands. The authors acknowledge the contribution from Dave Vogel for the implementation of control and the conduction of experiments The authors would also like to thanks the following companies for their support and technical advice in this project; Tecnotion B.V., Almelo, The Netherlands; Heidenhain Netherlands B.V., Ede, Netherlands, SigmaControl B.V., Barendrecht, The Netherlands.

References

[1] E. R. Laithwaite, S. A. Nasar, Linear-Motion Electrical Machines, Proceedings of the IEEE 58 (4) (1970) 531-540.

[2] D. M. Brouwer, J. P. Meijaard, J. B. Jonker, Large deflection stiffness analysis of parallel prismatic leafspring flexures, Precision Engineering 37 (3) (2013) 606-521.

[3] J. A. Haringx, The cross-spring pivot as a constructional element, Flow, Turbulence and Combustion 1 (1) (1949) 313-332.

[4] Tecnotion, Frameless Torque Motor Series (2018). URL https://www.tecnotion.com/downloads/catalogue-torque.pdf

[5] S. T. Smith, Flexures: Elements of Elastic Mechanisms, Taylor & Francis, London, 2000.

[6] S. Henein, Short Communication: Flexure delicacies, Mechanical Sciences 3 (2012) 1-4

[7] R. V. Jones, Some uses of elasticity in instrument design, Journal of Scientific Instruments 39 (1962) 193-203

[8] M. Naves. D. M. Brouwer, R.G.K.M. Aarts, Building Block-Based Spatial Topology Synthesis Method for Large-Stroke Flexure Hinges, Journal of mechanisms and robotics 9 (2017)

[9] J. B. Jonker, J. P. Meijaard, SPACAR – Computer Program for Dynamic Analysis of Flexible Spatial Mechanisms and Manipulators, in: Multibody Systems Handbook, Springer Berlin Heidelberg, Berlin, Heidelberg, 1990, pp. 123-143.